GreenFire Energy Closed-Loop Geothermal Demonstration using Supercritical Carbon Dioxide as Working Fluid

Alvaro Amaya[1], Joseph Scherer[1], John Muir[1], Mehul Patel[2], and Brian Higgins[1]

[1]GreenFire Energy, 4300 Horton Street, Unit 15, Emeryville, CA 94608
[2]Veizades & Associates, 5 3rd Street, Suite 400, San Francisco, CA 94103
alvaro.amaya@greenfireenergy.com, joseph.scherer@greenfireenergy.com

Keywords: closed loop, sCO$_2$, geothermal retrofit, demonstration, downhole heat exchanger, modeling.

ABSTRACT

GreenFire Energy has developed a geothermal power cycle that uses a closed-loop design with different working fluids. An experimental demonstration of this system has been performed at the Coso Geothermal Field with supercritical carbon dioxide (sCO$_2$) recirculated in a downhole closed-loop heat exchanger installed into an existing well. In this demonstration, sCO$_2$ was circulated through a 330-meter, tube-in-tube heat exchanger, hung from the wellhead. During testing, the well coproduced steam at seven different flow rates (including zero flow), combined with five different flow settings of circulated sCO$_2$. The development of a thermosiphon provided the motive force to circulate sCO$_2$. After the initial fill using the supply pump, no further sCO$_2$ pumping was required for continuous operation. A 1-D model was used to evaluate the experimental results. This model was developed by GreenFire Energy based on the conservation of mass and energy, considering heat transfer, friction, and the thermodynamic properties of the geothermal brine and circulating sCO$_2$. A finite-volume steady-state solution method was applied in the upflowing and downflowing directions, including heat transfer between flows, which required iteration to solve. Additionally, the coupling of the 1-D governing equations model and statistical techniques were applied to understand the experimental space domain, and different scenarios were simulated, allowing insight into how to optimize power production as a function of the principal operation variables and experimental design parameters. Experimental results show that a strong thermosiphon was easily achieved and could be varied by using the pressure control valve to either have peak pressure increase (with low flow) or high flow (with low pressure increase). Power potential was calculated using an isentropic efficiency assumption and it was found that peak power potential occurs at a balance between circulating sCO$_2$ flow rate and pressure rise by the thermosiphon. Other design variables, including sCO$_2$ temperature and length of closed-loop heat exchange, were simulated and analyzed using a Monte Carlo method. The primary goal of this demonstration was to verify GreenFire Energy's supercritical CO$_2$ process modeling assumptions and to illustrate the heat and power production potential of closed-loop geothermal technology under various operational conditions.

1. INTRODUCTION

Many hot potential geothermal locations lack sufficient porosity or water to be developed. Closed-loop geothermal projects can be used to address this shortcoming. A number of authors are investigating innovative closed-loop geothermal approaches (Hiroyuki et al., 2019; Law et al., 2014; Higgins et al., 2016). One reason for considering closed-loop geothermal is to reduce drilling risk by retrofitting existing wells (Higgins et al., 2019). Another advantage is to reduce geothermal emission issues experienced with geothermal brine properties at some sites (Yanagisawa et al., 2017; von Düring et al., 2016). Using CO$_2$ as working fluid in geothermal systems is also investigated by others (Guo et al., 2019; Oldenburg et al., 2016). This research considers these important topics in a field-scale demonstration, including the thermodynamic and statistic process modeling.

GreenFire Energy has shown in previous modeling analyses that resources with hot, dry rock can be economically developed using closed-loop heat extraction technologies (Fox and Higgins 2016; Higgins et al., 2016; Higgins et al., 2019). GreenFire Energy has demonstrated how a down borehole heat exchanger (DBHX) can be used in new projects that extract enthalpy from deep wells in hot, dry rock. Verification of GreenFire Energy's modeling will help the future development of approaches to retrofit existing hydrothermal wells to become productive and to plan and build full-scale, closed-loop geothermal projects using wells drilled into hot, dry rock.

2. THE DBHX CLOSED-LOOP TECHNOLOGY

GreenFire Energy's DBHX is simply a tube-in-tube assembly installed into an existing well. The DBHX is hung from the existing wellhead with modifications so that the working fluid can flow in and out of the DBHX independent from the production of geothermal fluid. The DBHX consists of a liner inserted into the well with a plugged end at the lowest point. The geothermal resource is allowed to flow around this liner and may, or may not, be produced to the surface. Inside the plugged liner, a vacuum insulated tube (VIT) is installed, extending nearly to the bottom of the liner. When using supercritical CO$_2$ (sCO$_2$) as the working fluid, the optimal flow direction is downward through the inside of the VIT, returning in the annular region between the VIT and the liner (Figure 1). This same demonstration facility was used to evaluate water as the working fluid, which was published previously (Higgins et al., 2019).
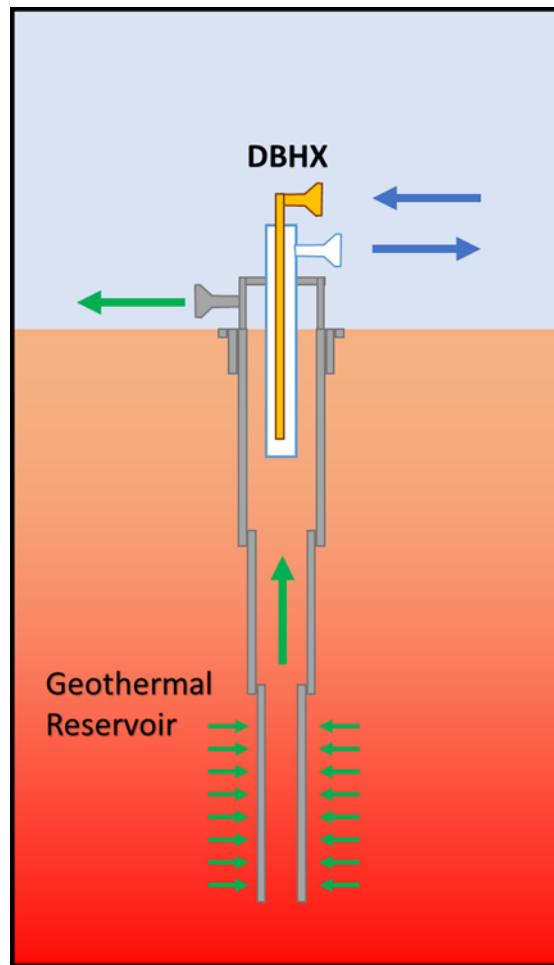
Figure 1: A schematic showing the DBHX. The blue arrows indicate the flow of sCO_2 (inlet to the center of the VIT and outlet from the annular region of the DBHX). The green arrows indicate the flow of geothermal brine to the surface around the DBHX.

3. EXPERIMENTAL PROCESS FLOW DESCRIPTION FOR SCO_2

In Figure 2, a process flow diagram (PFD) is shown with sCO_2 (black) as the working fluid in the DBHX. The flow direction for sCO_2 in the DBHX is down the center of the VIT and up the annular portion of the DBHX. By flowing in this direction, the sCO_2 retains high density all the way to the bottom of the DBHX, and this allows a strong thermosiphon to be built, maximizing the sCO_2 enthalpy production to the surface.

Also shown in Figure 2 is the flow of coproduced the geothermal brine (green) and the cooling water (blue) required to reject excess heat from the circulating sCO_2.

Due to cost and schedule, a supercritical expander (turbine) with a generator was not used in this study to directly generate power. Instead, the sCO_2 was expanded across a control valve. The thermodynamic state of the sCO_2 before and after the control valve is used along with the measured mass flow rate to calculate the power that would be generated had a turbine been installed.

Three control parameters can be varied in this arrangement: (1) the flow rate of geothermal brine produced to the silencer (using the green PCV), (2) the flow rate of sCO_2 through the closed-loop system (using the black PCV), and (3) the flow rate of cooling water (using the blue PCV). Generally, the well flow (green PCV) was set first and the well was allowed time to come to equilibrium. Then the sCO_2 flow control valve was stepped from 100% to 20% open in four or five steps. The cooling water control valve is used to control the returning (injection) sCO_2 temperature.
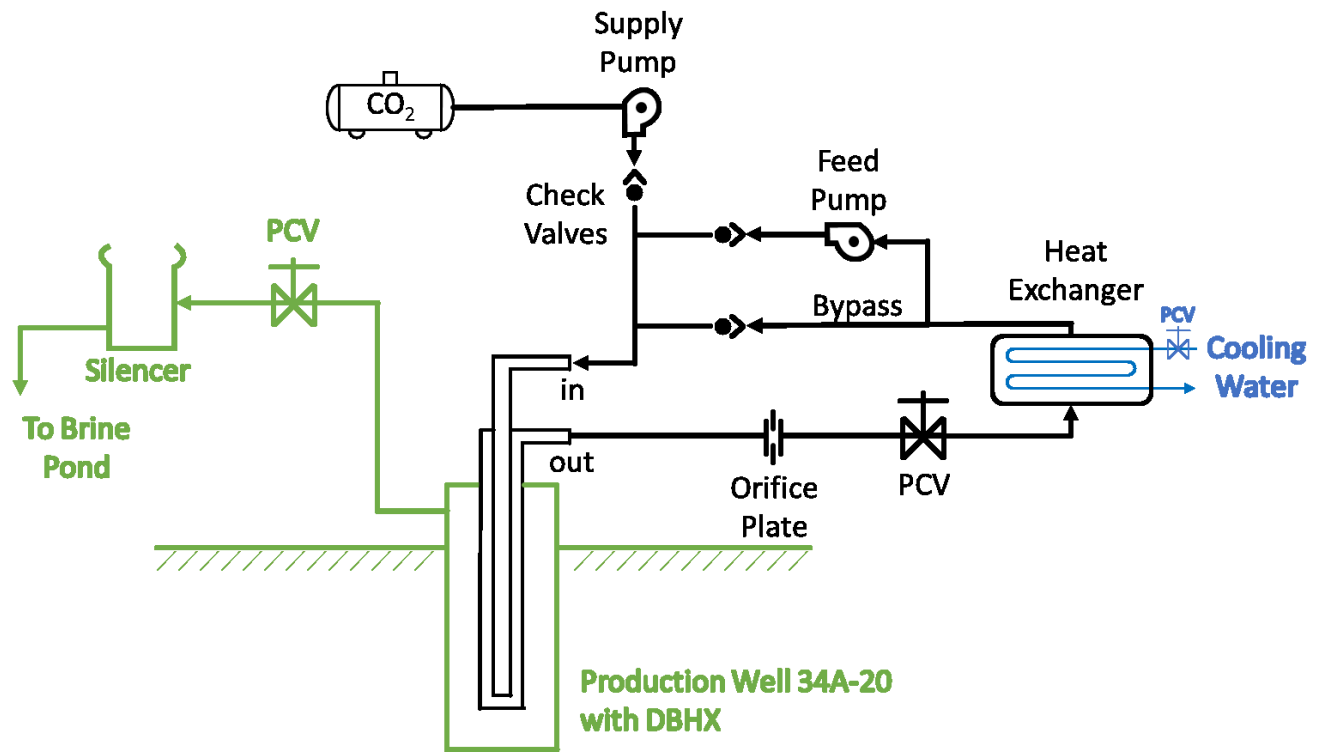
Figure 2: The DBHX process flow diagram for sCO$_2$ as the working fluid. The sCO$_2$ flow is shown in black; the cooling water flow is shown in blue, and the geothermal fluid is shown in green.

During testing, the flow of geothermal fluid to the silencer was hand analyzed for (1) flow rate of steam, (2) flow rate of brine, and the (3) NCG content in the steam. From this data and pressure, the resource enthalpy was deduced. For test data not corresponding to a physical flow analysis, a two-phase orifice plate correlation was used to evaluate the geothermal brine flow characteristics. The flow rate of sCO$_2$ through the closed-loop is measured using an orifice plate with a differential pressure measurement.
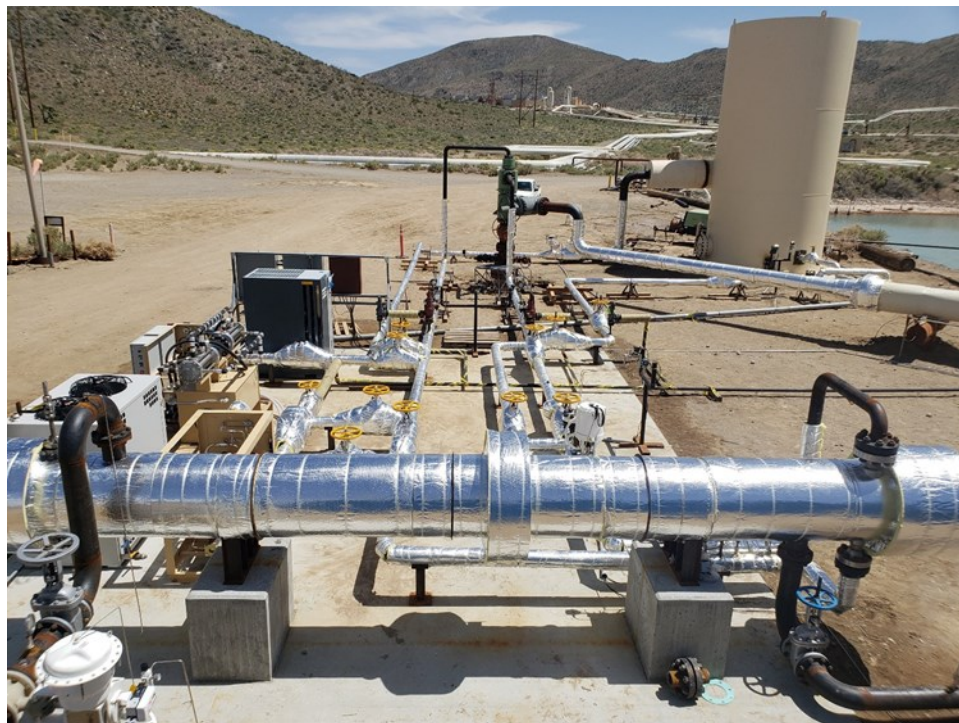

Figure 3: Photo of the demonstration surface equipment.

Figures 3 and 4 show the demonstration surface equipment. In the foreground of Figure 3 is the heat exchanger. Just past the heat exchanger on the left side (front to back) is the feed pump, the chiller (to keep the supply pump from prematurely vaporizing the CO_2 while it is loaded), the supply pump, the air compressor (used to power the feed pump), and the electrical panel. In the center background of Figure 3 is the well with three connections (top to bottom): the VIT inlet, the DBHX outlet, and the well outlet (to the atmospheric flash tank shown in Figure 4). The insulated pipe works in the middle of the picture with the yellow-handled valves, make up the rest of the surface equipment. The DBHX outlet flow PCV is just visible on the right side just beyond the heat exchanger. The flash tank and piping beyond the wellhead were used in the water-as-working-fluid testing, presented previously (Higgins et al., 2019).

The supply pump was used only to fill the piping and DBHX with sCO_2 from the insulated CO_2 receiver holding tank. The feed pump was provided to start the sCO_2 thermosiphon in case it stopped. In practice, due to the check valves, the simple action of adding sCO_2 to the system was enough to initiate the thermosiphon, which never stopped during testing.

Figure 4: Photo of the demonstration equipment just after the well was opened with CO_2 being pumped into the closed-loop system.

Figure 4 shows the demonstration equipment during testing when the well was producing to the atmospheric flash tank in the background. The blue water tanks were used to hold cooling water for the testing. In the center of Figure 4 is the CO_2 supply pump in operation during startup and commissioning. The photo in Figure 3 was taken from atop the blue water tanks in Figure 4.

4. PROCESS MODELING FOR SCO$_2$ AS WORKING FLUID

4.1 Modeling the Surface Equipment

In the full-scale application, the above-ground surface equipment comprises a turbine (or expander), heat rejection, and an optional feed pump (compressor). For the demonstration, the turbine was simulated using isenthalpic expansion across a control valve, and the compressor was only sized to start the cycle; that is, it only could handle a portion of the expected flow. Once the thermosiphon establishes itself, the circulating CO_2 bypasses the pump. To model the surface equipment, we use an isentropic efficiency assumption for the turbomachinery; typically, commercially available in a range from 80% to 85%.

In a full-scale application, the heat rejection is generally modeled using either ambient air or an evaporative water-cooling system, taking into account local ambient weather conditions (temperature, pressure, and humidity). For this work, a large water reservoir was used as a heat sink for the installed heat exchanger.

4.2 Closed-Loop Modeling

We use a 1-D process model built in MS Excel to model the steady-state, closed-loop flow. This model takes into account conservation of mass and energy, and includes isentropic compression and expansion as the sCO_2 moves up or down the well. Friction is accounted for in the well using a Darcy friction factor via the Haaland equation (Haaland, 1983). Friction manifests itself in the model as pressure drop. Heat transfer is modeled as 1-D conduction through solid sections and as convection to fluids using a Nusselt number calculated with the Dittus-Boelter equation (Bergman, 2011). Heat loss to the overburden was considered to be small and was not modeled. Gas and liquid properties are called from the NIST database using CoolProps, an Excel plugin (Bell et al., 2014).

A one-dimensional, finite-volume, steady-state implicit solution scheme is used to solve the equations described above (similar to the Euler Method, see for example Griffiths and Higham, 2010). For each small length interval, the "next" position is calculated using two thermodynamic variables from the previous length interval, from which all other thermodynamic variables are calculated using the current position. By using a sufficiently small length interval, this solution method converges to the explicit solution.

There are three flows to be considered: the downflowing closed-loop fluid, the upflowing closed-loop fluid, and the coproduced geothermal fluid. The boundary conditions are defined for the inlet of each of the three flows according to temperature, pressure, and flow. Heat transfer from the geothermal brine to the working fluid in the closed-loop, as well as through the VIT (between the upflow and downflow working fluid) is also considered. Because the upflowing closed-loop fluid conditions are equal to the exit conditions for the downflowing closed-loop fluid (as the fluid "turns the corner"), the solution requires iteration. Worth noting is that the VIT does not have a continuous internal nor external diameter due to having a joint every 10 meters. To account for this disruption to the flow in the friction calculation, we model the VIT with a slightly smaller inside diameter and a slightly larger outside diameter (e.g., ~10%). More details can be found in our previous works (Fox and Higgins, 2016; Higgins et al., 2016).

Additionally, a principal component analysis (PCA) and Bayesian statistics modeling techniques were applied to the experimental data results in this study to optimize an objective function of power production as a function of system variables directly related to the flow measurements such as the wellhead pressure for the well side, and the DBHX differential pressure for the closed-loop system side. The power production function has been contrasted and validated by using a coupling between the thermodynamic 1-D process model system equations and a Monte Carlo simulation methodology to produce a statistic modeling forecast including other key variables (i.e., DBHX length, sCO_2 inlet temperature, and sCO_2 flow rate).

5. RESULTS FOR SCO_2 AS THE WORKING FLUID

There were two onsite demonstration periods during which sCO_2 was tested: May 2019 and December 2019. First the data from May 2019 are presented. In May 2019, the well was cycled through three different production rates: low, medium, and high (described below). Likewise, the closed-loop was circulated with five different control valve settings (20%, 40%, 60%, 80% and 100%). In total, 15 combined flow setting conditions were investigated as shown in Table 1.

Table 1: Well and closed-loop test conditions

Test numbers	Well Flow (kg/s)	Closed-Loop PVC Set Point (%)
A1-A5	20.0	100, 80, 60, 40, 20
B1-B5	13.0	100, 80, 60, 40, 20
C1-C5	5.4	100, 80, 60, 40, 20

5.1 Well Flow Data

Well flow data from several tests are plotted in Figure 5, showing the measured wellhead pressure (WHP-left) and wellhead temperature (WHT-right) versus the well flow (measured in the brine collection system using an orifice plate with a two-phase flow correlation). The orange symbols are the temperature measurements and the blue symbols are the pressure measurements. The data measured during the sCO_2 testing are displayed in crosses and asterisks respectively, brine measurements are displayed in opened square and round symbols respectively, non-closed symbols were measured in 2019 while testing the DBHX with a second working fluid, the closed symbols represent measurements made in 2018 before the DBHX installation, and DBHX-temperature for water and sCO_2 are displayed in red-opened diamond and triangle symbols respectively. Some of the well flow data from our testing with water as the working fluid is included in Figure 5 to show the consistency of the well (Higgins et al., 2019). Generally, the well production was similar during sCO_2 testing as compared to previous testing. This well currently produces saturated steam with high levels of non-condensable gases (NCGs), averaging 20% to 25% by weight.
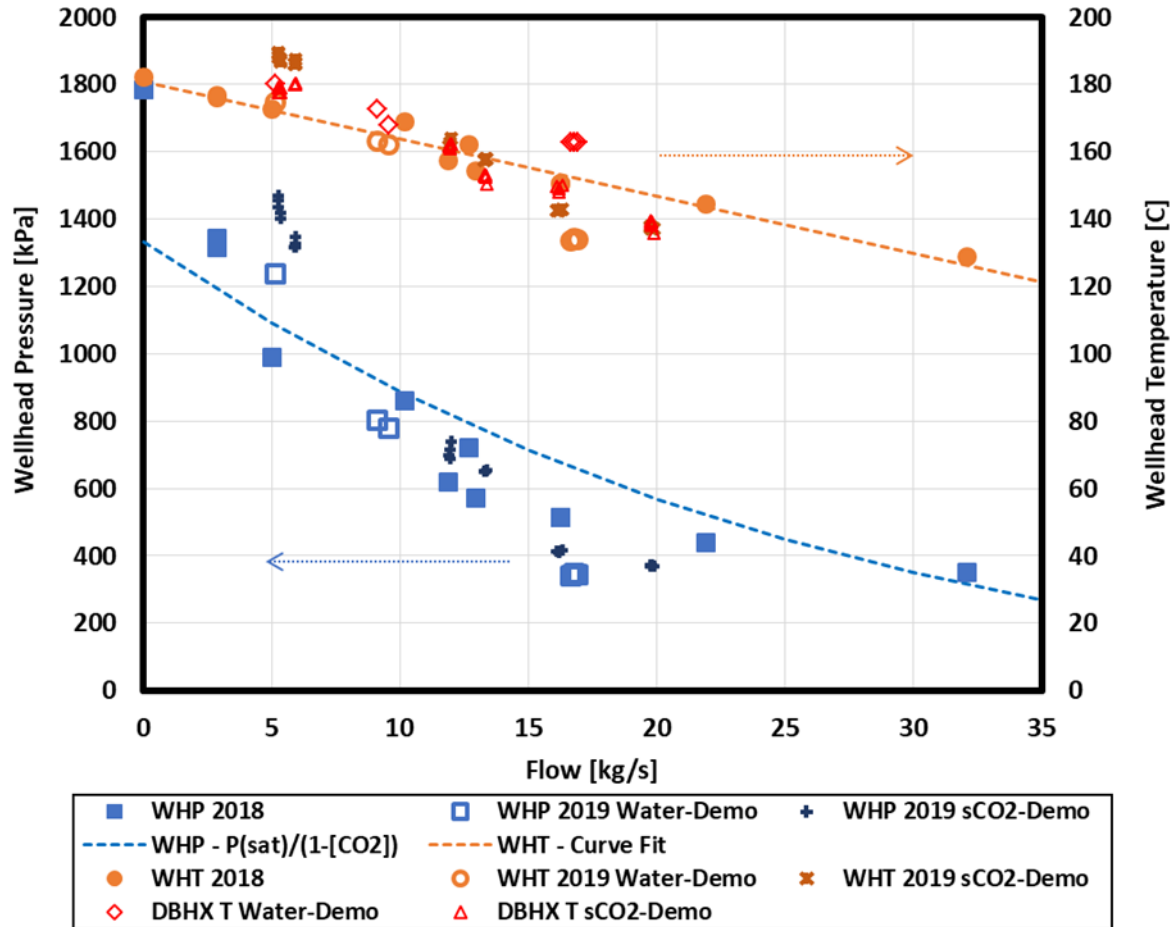
Figure 5: Geothermal production wellhead pressure (WHP – left) and wellhead temperature (WHT - right) plotted versus well flow. The dashed line is a linear curve fit to the temperature. The solid line is the saturation pressure (including NCGs) calculated at the curve-fit temperature.

Generally, as shown in Figure 5, as the well is closed in, the flow rate of the produced stream is lowered, at the same time, the wellhead pressure and temperature increase. A curve is fit through the data of wellhead temperature versus flow rate (orange dotted line). For each temperature, the saturation pressure is calculated and plotted versus flow rate (blue solid line). This saturation pressure accounts for the 23% CO_2 concentration in the well flow. These two lines demonstrate that, as expected, the increase in wellhead temperature for lower well flow happening due to the saturation temperature of the well at the increased wellhead pressure (accounting for the NGCs). Figure 5 also shows that the expected decay of pressure and temperature of the well as a function of the brine extraction flow in 2018 (prior to the demonstration of the closed-loop DBHX system at Coso) has the same characteristics as when tested during the closed-loop system demonstration. Therefore, heat extraction is sustainable so long as the upgoing conductive heat flow of the system is equal or less than the energy extracted.

5.2 Well Flow Data during Closed-Loop DBHX Demonstration While Flowing sCO$_2$

Figure 6 shows the geothermal resource wellhead pressure (WHP) and temperature (WHT) plotted as a function of the well flow data from Tables 1 and 2. This figure confirms that the well flow, while slightly different from May 2019 to December 2019, has not fundamentally changed in its enthalpy or wellhead delivery.

In Figure 7, power is plotted versus the increase in temperature (left) and pressure (right) across the DBHX. To calculate the electric power potential of the circulating sCO$_2$, we use a simple isentropic efficiency assumption. In this assumption, we included an assumed pressure drop required through a full-scale installation of the surface equipment (primarily the heat exchanger). We based the turbine inlet thermodynamic conditions on the measured pressure and temperature of the sCO$_2$ exiting the DBHX. At the outlet of the turbine, we use an 80% isentropic efficiency calculation for the turbine work, combined with a turbine outlet pressure equal to the DBHX inlet pressure plus 70 kPa (~10 psi) to account for the heat exchanger and piping pressure drop.
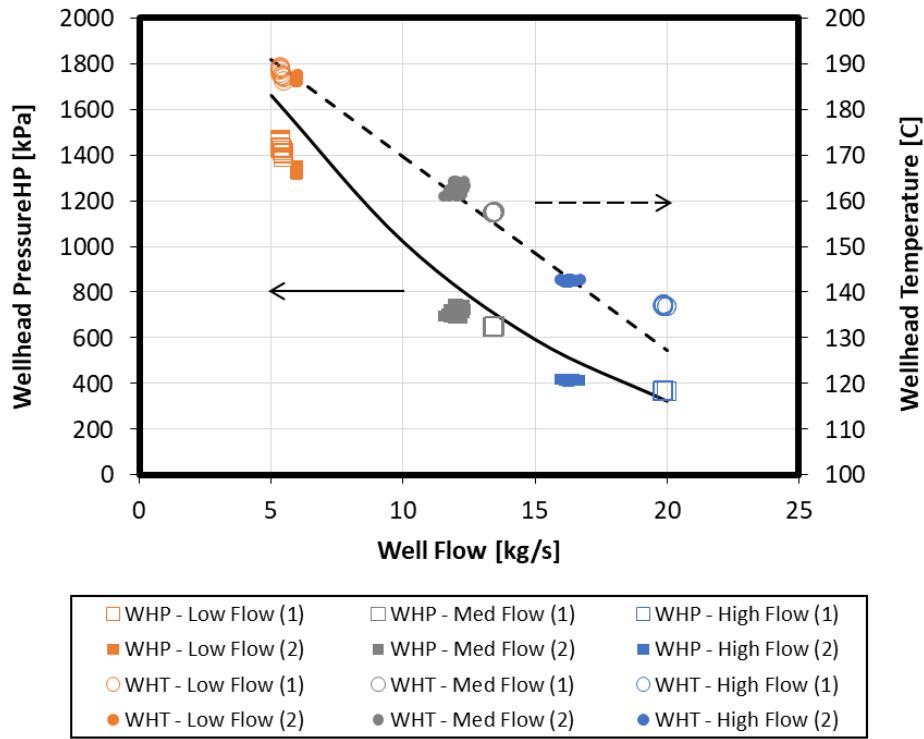
Figure 6: WHP (square symbols) and WHT (round symbols) opened symbols for the May 2019 demo (1), and closed symbols for December 2019 demo (2) of the geothermal brine plotted versus the geothermal produced flow. The dashed line is a linear curve fit to the temperature. The solid line is the saturation pressure (including NCGs) calculated at the curve-fit temperature.
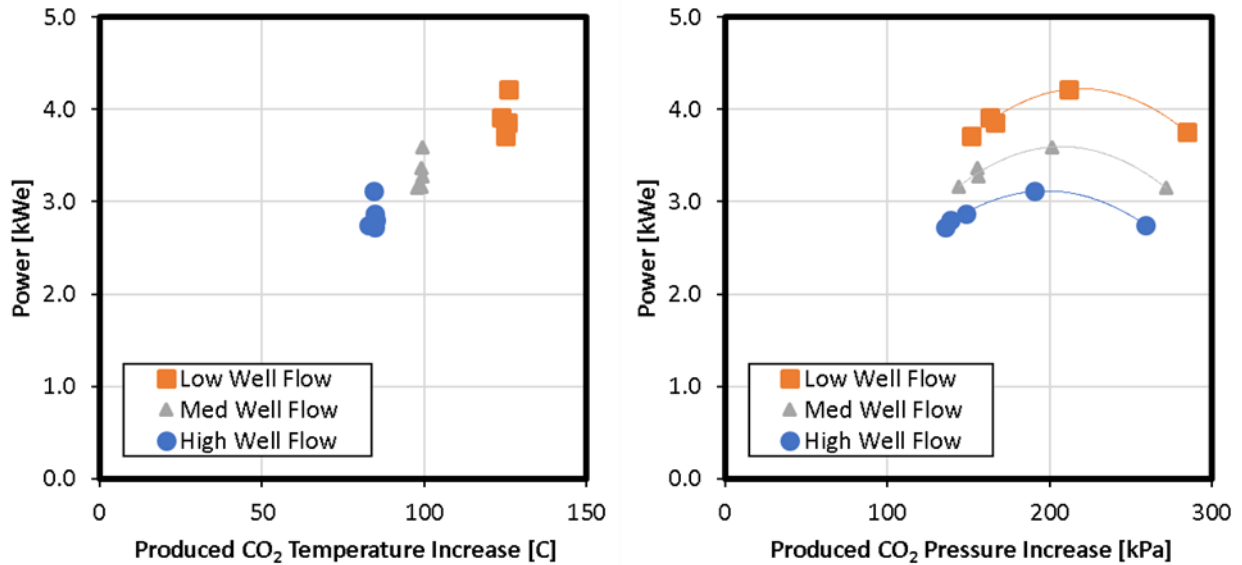

Figure 7: Electric power production potential for the DBHX sCO$_2$ flow plotted versus (left) the produced sCO$_2$ temperature and (right) the produced CO$_2$ pressure increase. The average DBHX inlet temperature and pressure were 36°C and 7700 kPa. The lines in the right panel are simple parabolic curve fits to visualize the trends.

As expected from the modeling, and as clearly shown in Figure 7, more power is produced when the rate of coproduced geothermal fluid is reduced (i.e., "Low Well Flow"). This raises the temperature of the geothermal fluid that meets the closed-loop downhole heat exchanger, allowing the heat exchanger to absorb more heat. Additionally, and also corresponding to the modeling, more power is not produced when the Produced CO$_2$ Pressure Increase is highest. This is because a high pressure increase is associated with a substantially

lower circulation rate of sCO$_2$ within the DBHX. The highest power production is a balance between a high DBHX circulation rate and high produced differential pressure.

Unfortunately, due to a disruption in freshwater availability, the sCO$_2$ return temperature at the inlet of the DBHX was 36°C when it should have been much closer to the critical point temperature (31.1°C). This 5°C temperature difference near the critical point reduced the sCO$_2$ density by nearly 60%. The reduced density reduced the formation of the thermosiphon and resulted in less power than expected. This is discussed in more detail later.

5.3 Zero Well Flow Data

One of the goals of the testing was to determine the heat extraction and power production for conditions where the well was not flowing. It was expected that without brine flow in the well, conditions would approximate those in hot, dry rock. Consequently, at the end of the experiment, the well was shut in and the sCO$_2$ within the DBHX was allowed to continue flowing until the well cooled. In Figure 8, each black/yellow diamond represents a rolling average of five-minute data as the well cools off over about one hour. Just before the well was shut in, the flowing conditions were hottest (low well flow, shown by the orange squares, produces the hottest condition). The first zero well flow conditions (when the well was hottest) are the data with the highest power estimates (~4.2 kWe). When the well is no longer flowing, the heat that is extracted by the DBHX comes from the residual heat in the well casing and the steam and brine in the annular region between the well and the DBHX.
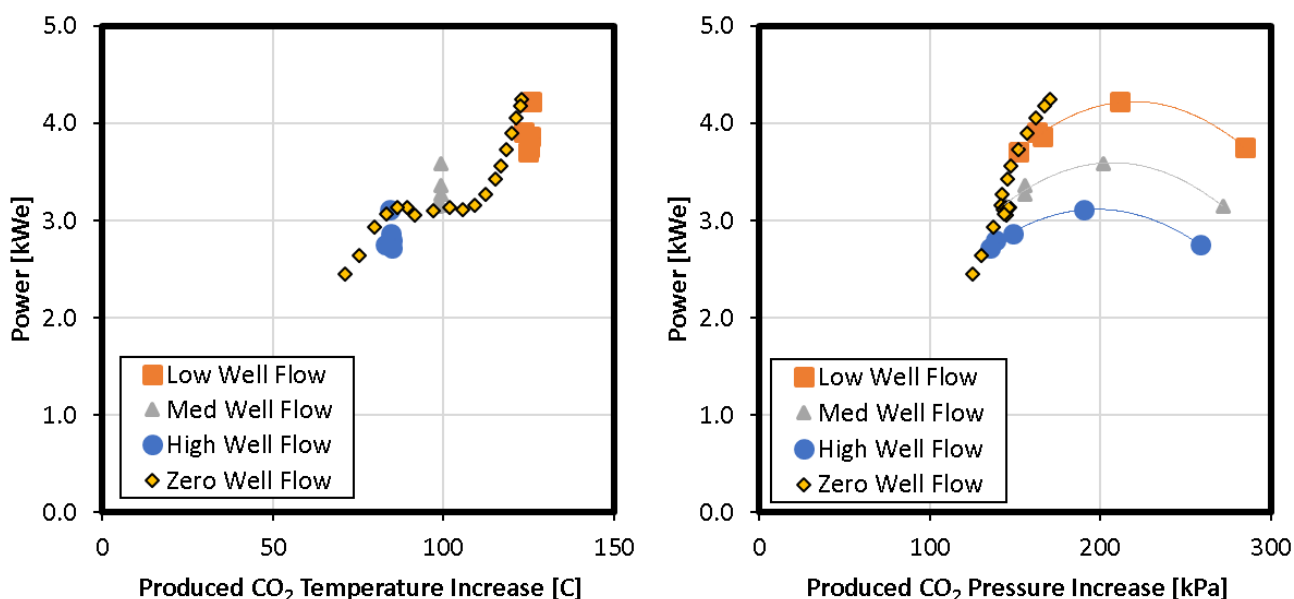

Figure 8: This is the same data from Figure 7, with the added data from the zero-flow test (black/yellow diamonds).

5.4 Well Flow Modeling

In December 2017, during the well productivity testing, downhole flowing and static surveys were performed without the DBHX in place. The <u>measured</u> downhole temperature and pressures are plotted in Figure 9 using dotted lines. As expected, both the temperature and pressure are lower when the well is flowing unobstructed and at a high rate.

Also, in Figure 9 are <u>modeled</u> downhole temperatures and pressures for several well flow conditions corresponding nominally to the conditions in Table 1 (orange for high, yellow for medium, and green for low well flow). The bold orange line ("High Well Flow") is the modeling data that corresponds to the flowing well survey. Both the temperature and pressure follow the measured values. Likewise, the bold blue line ("Static") is the modeling data that corresponds to no flow being produced by the well. Again, both the downhole temperatures and pressures closely match the measured values. For the mid- and low-flow cases, only surface temperature and pressure were measured and the plotted data in Figure 9 represent modeled data only.

For each of the well flow conditions in Table 1, the closed-loop flow was modeled while also modeling the geothermal flow. Figure 9 shows one such condition, corresponding to the highest power potential modeled. The bold black lines in the right image in Figure 9 are the temperature within the DBHX, showing a very small temperature rise as the sCO$_2$ flows downward inside the VIT and a large temperature rise as it flows back up the annular region between the VIT and the DBHX outside liner. Due to the flow direction, the geothermal brine and sCO$_2$ leave at approximately the same temperature (compare the top of the red and black lines in the right figure).
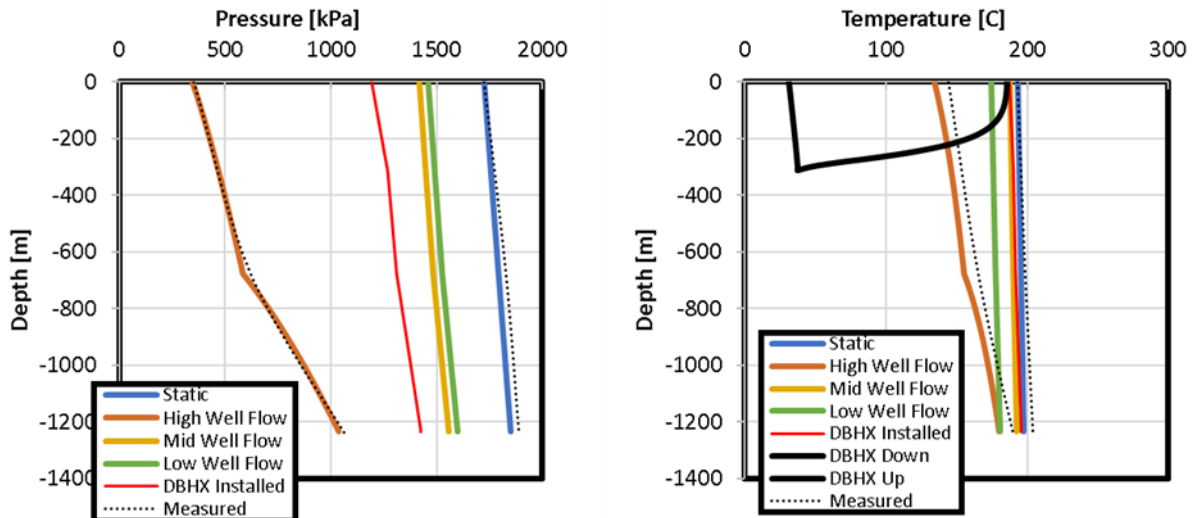
Figure 9: Temperature and pressure versus depth with the DBHX modeling for one test case.

5.5 Demonstration Results versus Modeling

Each data point from the demonstration (i.e., Table 1) was modeled. Additional points were also modeled considering higher and lower sCO$_2$ flowrates through the DBHX. These measured data (as points) and predictions (as lines) are plotted in Figure 10. These images together again show that the maximum power is not produced by the maximum recirculation rate of sCO$_2$ through the DBHX nor is it produced when the thermosiphon is strongest. Rather, the maximum occurs at a point between the maximum circulation rate and maximum thermosiphon pressure production.
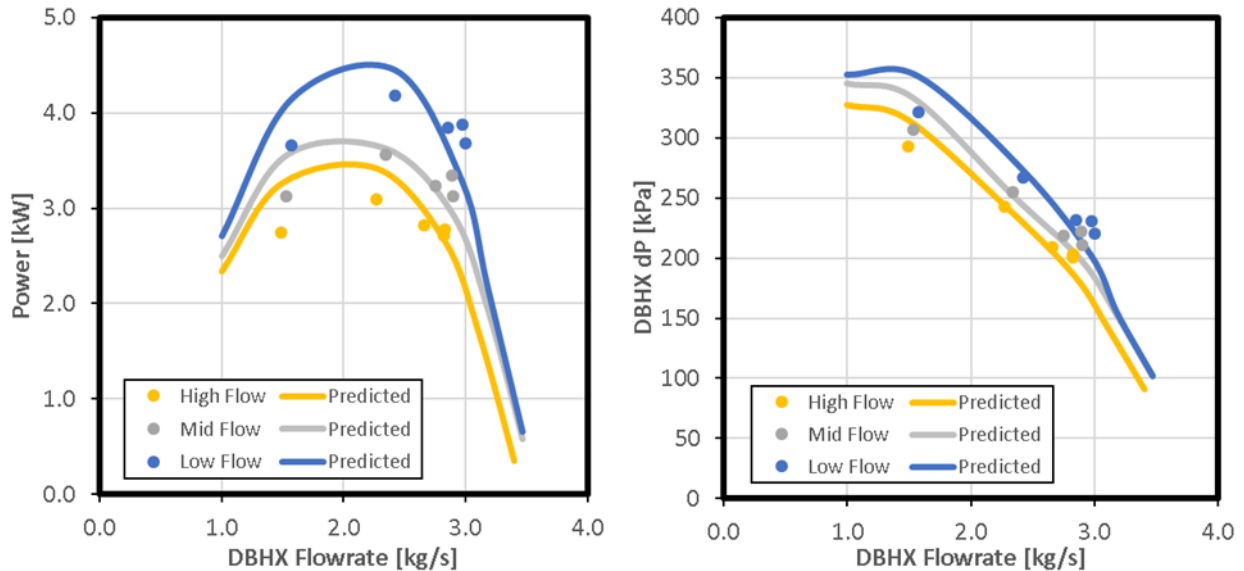

Figure 10: Power production calculated from the sCO$_2$ thermodynamic conditions and modeling data plotted versus the sCO$_2$ flow rate (left) and measured and calculated pressure rise across the DBHX versus the sCO$_2$ flow rate (right). Colors indicate the well flow conditions in Table 1.

As an indication of how well the modeling compares to the measured data, the modeled datapoints are plotted versus the measured points in Figure 11 (noting that "measured power equivalent" is calculated using the enthalpy difference as described above). Generally, the predicted data follows the measured trends.
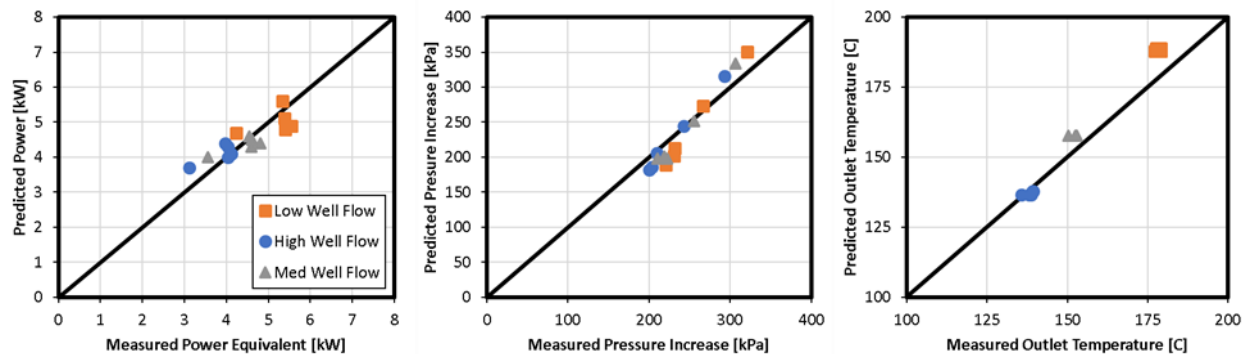
Figure 11: The predicted power (left), pressure increase (middle), and temperature (right) rise plotted versus the measured values. The measured power is calculated directly from measured thermodynamic data as described in the text.

5.6 Modeling Lower Injection Temperature and Deeper Wells

Due to conditions outside of our control, the water available to operate the heat exchanger was not as cool as would be expected from the cooling tower water supply. The water we ended up using during the testing was sourced from a nearby sump. As such, the coldest we could return the sCO_2 back to the DBHX was 36°C. CO_2 near the critical point (31.1°C) is quite dense and properties vary widely with just a small change in temperature. For example, at 7.5 MPa, the density of sCO_2 at 31°C and 36°C is 614 kg/m^3 and 261 kg/m^3, respectively. This large reduction in density results in a far smaller thermosiphon effect in the May 2019 testing than in the December 2019 testing.

A second modification that we considered, but did not implement due to costs, was to make the DBHX longer (i.e., extending deeper into the well). The installed system was 330 m deep, and we have looked at "what if" the DBHX was 1000 m.

To illustrate the effects of a colder injection temperature and also a deeper DBHX, we have repeated the modeling using these new conditions and have plotted this in Figure 12 against the data presented above.
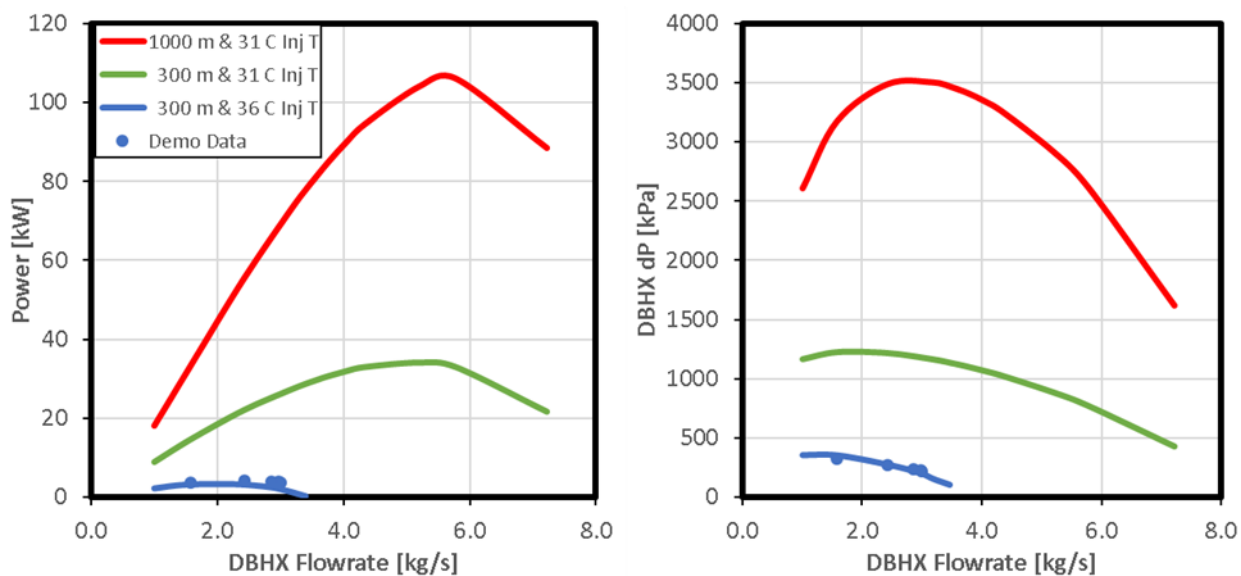

Figure 12: Power production (left) and pressure rise (right) plotted versus the DBHX flow rate for three different DBHX operational scenarios.

In order to better understand why there is so much more power produced for these two changes (colder sCO_2 inlet temperature and a deeper DBHX), Figure 13 shows the predicted temperature, pressure, and density of the sCO_2 as it recirculates through the DBHX. In this figure, dotted lines represent downflow and solid lines represent upflow. The data plotted is for the peak power production case for the three scenarios. In blue is the data matching the demonstration, in green is the same depth but with a colder inlet temperature, and in red is the deeper well (also with a colder inlet temperature).
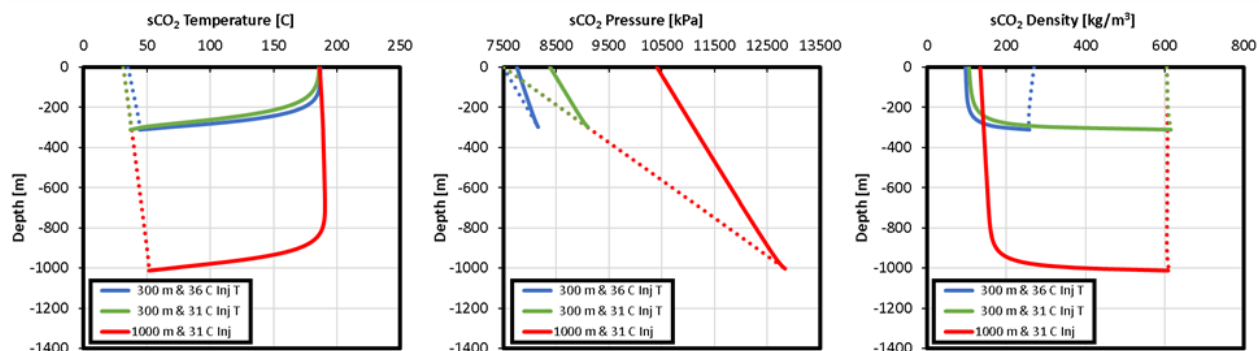
Figure 13: The predicted downhole temperature (left), downhole pressure (middle), and downhole density (right) of the circulating sCO₂ are plotted versus depth for three different DBHX scenarios. The dotted lines indicate downflow and the solid lines indicate upflow.

Consider the rightmost figure first. This shows the density of the sCO_2 as it recirculates through the DBHX. The dotted blue line shows that under the demonstration conditions the density is around 260 kg/m^3 as it enters. It slightly loses density as it reaches the bottom of the VIT (due partly to heat transfer through the VIT, which is not entirely adiabatic and largely to frictional pressure losses). The red and green lines show injection at the lower temperature (higher density) and here the density does not change as much as the sCO_2 descends the VIT. Since the density is so much higher at the lower temperature, the velocity is proportionally lower and therefore there is less frictional pressure loss (hence a more vertical line). As the sCO_2 returns to the surface, the deeper well produces more pressure, and this is seen in the red line as a higher density at the surface (even through the returning temperature is similar).

The middle image in Figure 13 shows the cumulative pressure built up as the sCO_2 descends the VIT and the pressure loss as the less-dense sCO_2 returns in the annular region of the DBHX. The higher inlet temperature (blue) doesn't build up as much pressure. The lower inlet temperature does (red and blue) and the deeper DBHX builds up a lot more pressure (red).

5.7 Retesting sCO₂ at Lower Inlet Temperature

Because the sCO_2 inlet temperature at the DBHX was hotter than desired during the May 2019 demonstration, GreenFire Energy retested the circulation of sCO_2 as a working fluid in December 2019. This testing sequence followed a very similar testing plan.

Data are presented in Table 2 below for the closed-loop DBHX flowing with sCO_2 while producing the well in December 2019. The well was cycled through three different brine production rates: low, medium, and high as shown in Table 2 below. These are slightly different from Table 1, as seen in Figure 6. The sCO_2 was circulated in the DBHX with four different control valve settings (20%, 40%, 60%, and 100%). In total, 12 combined flow conditions were investigated.

Table 2: Well and closed-loop test conditions (December 2019)

Test numbers	Well Flow (kg/s)	Closed-Loop PVC Set Point (%)
D1-D4	6.0	100, 60, 40, 20
E1-E4	12.0	100, 60, 40, 20
F1-F4	16.3	100, 60, 40, 20

Figure 14 shows that the measured power production was several times higher during the retesting. As was shown previously, more power can be generated when the rate of coproduced brine is reduced (i.e. "Low Well Flow"); however, the effect is not as pronounced as seen in the May 2019 data.
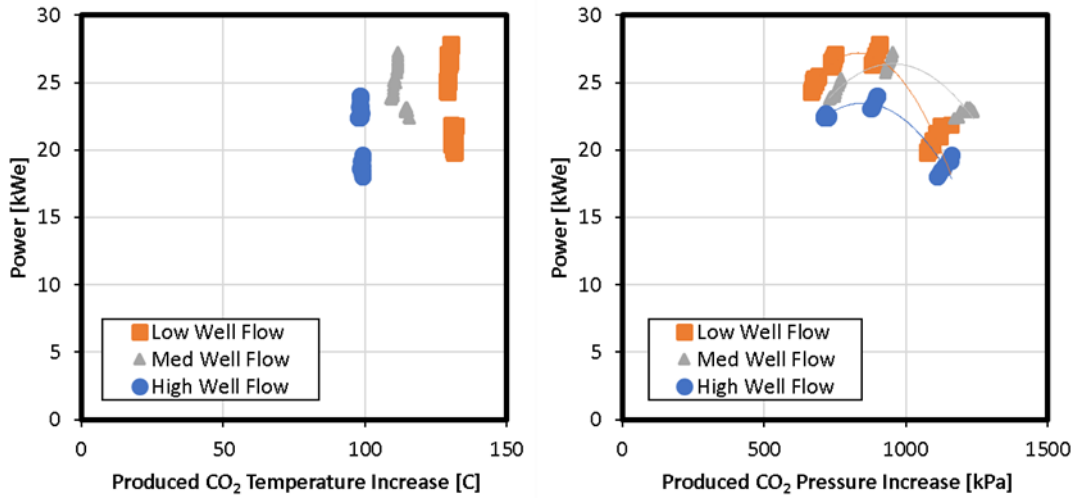
Figure 14: Power production vs. increased temperature and pressure.

The newly measured December 2019 data are next plotted in Figure 15 (which can be directly compared to Figure 12) and match well with the previously modeled data.
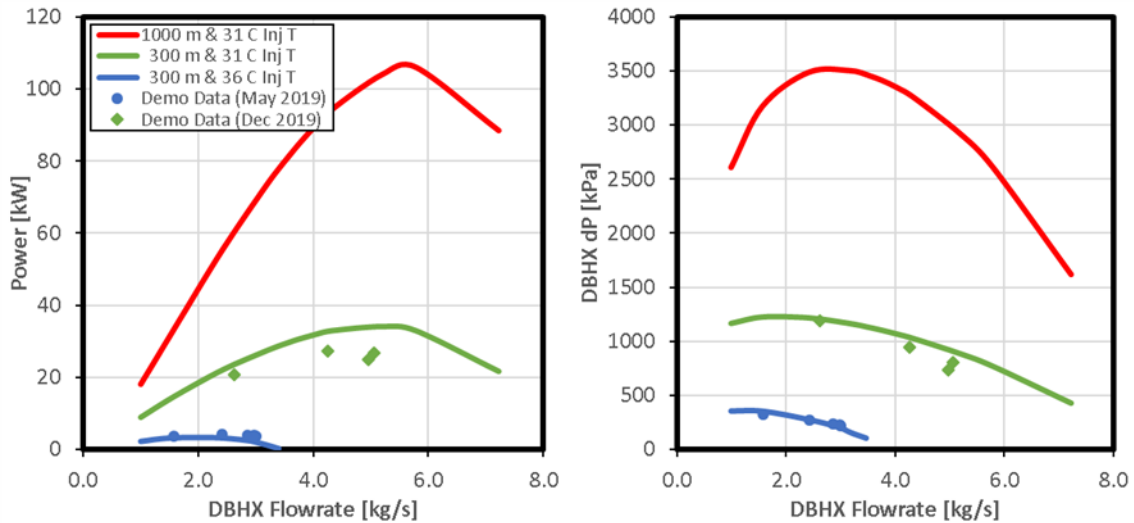

Figure 15: Estimated power production with amended conditions.

During the December 2019 testing, the "zero flow case" was tested on a different day from the well flow testing. In Figure 16, each black/yellow diamond represents an average of 30 seconds of data. The line shows the progress of the data as the well cools for about twenty-two minutes while the flow rate was increased. This data is plotted (along with the well flow data) in Figure 16. As seen previously, the highest power potential is at the beginning (shortly after the well is shut in), and it tapers off over a 30-minute period as heat is extracted. Figures 8 and 16 suggest that the zero well flow data and the verified modeling can also be used to estimate power potential from hot, dry rock.
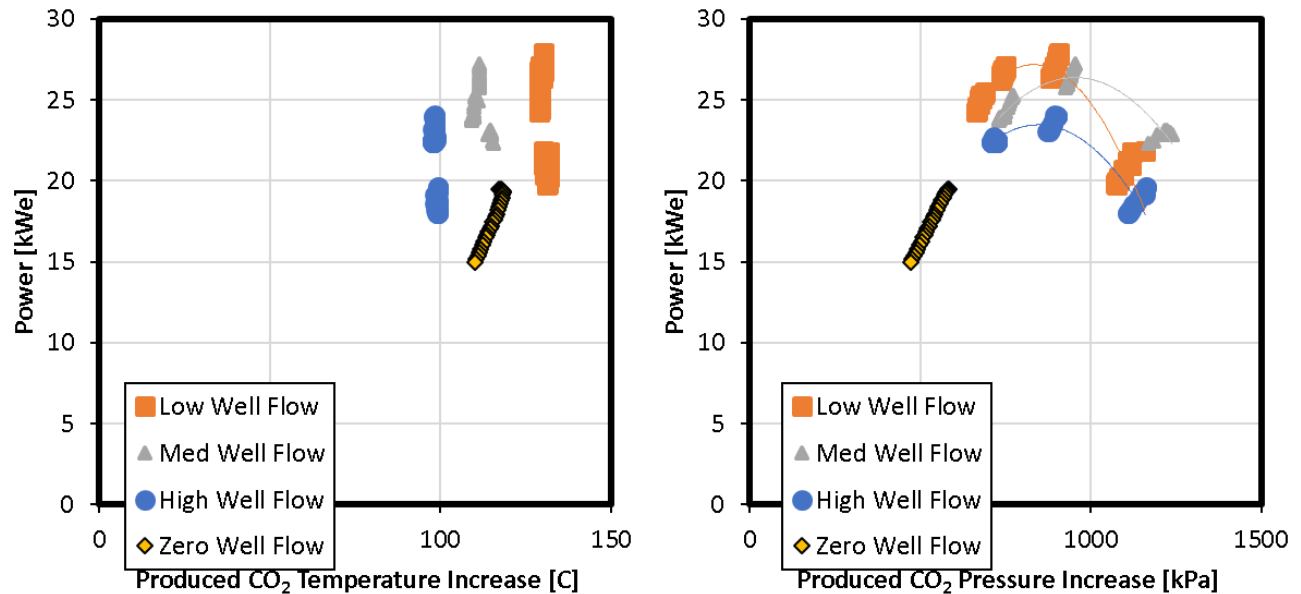
12

Figure 16: This is the same data as Figure 14, adding in the zero well flow data (black/yellow diamonds) taken a day earlier.

5.8 Statistical Modeling

In order to determine optimal flow under the tested conditions, statistic modeling methodology using principal component analysis (PCA) and Monte Carlo simulation method was carried out for two scenarios: optimization for power production, and optimization for heat recovery.

PCA is a statistical technique that transforms all the variables and all the experiments (observations) into dimensionless vectors and scores them. The PCA vectors create new axes where the integrated information can be plotted and optimally analyzed.

Figure 17 is a PCA biplot graph that displays variables and observations position at the same time. Loadings and scores are plotted together on the same principal component axes defined by system variables directly related to the flow measurements for specific sCO_2 and brine well control valve settings such as the wellhead pressure for the well side and the DBHX differential pressure for the closed-loop system side. Over the spatial domain, the power production function has been contoured (see Figures 17a and 17b) to show in the same graph 98% of the variance information based on 28 observations and 32 variables.

The statistical modeling processes consist of five steps:

In the first step, the twenty-eight experimental sets (each of them represented by 32 operational variables) were analyzed. Principal component 1 (52.6% of variance) and principal component 2 (45.1% of the variance) comprise 97.7% of all the information (see axes in Figure 17).

In the second step of the analysis, the PCA axes are correlated with specific variables that explain the orthogonal space where the variables and the experiments should be placed as vectors (red lines) and blue dots (represent the observations or experiment scores that are labeled as A_i-F_i respectively). Following a multifactorial analysis should find the principal variables that govern the experiment behavior. In this case, Wellhead Pressure and ΔP DBHX sCO_2 were the main variables that controlled the experimental processes and those variables define the axes in Figure 17.

In the third step, the orthogonal dimensionless space is created through a power [kW] equation (see the contours in Figure 17a) and heat [MW] equation (see the contours in Figure 17b). These contours overlay the experimental space domain, show the position of tests, observations and variables orientation (vectors defined by its magnitude, direction, and angles) related to power optimization direction and show the power magnitude on the spatial domain.

The fourth step is an integrated analysis that produces optimized values within the experimental domain which maximizes the power production function with the relevant information obtained from all the experiments. The power source energy (over layered as a function in Figure 17a) produced less than 5% error in its estimation for all the twenty-eight experimental test conditions (A_i-F_i). Figure 17b shows the same principal component analysis and factors but with heat energy contours. The available heat from the DBHX is more than 50 times higher than electrical power creating an attractive potential for the delivery of heat for commercial purposes such as mineral extraction industry from geothermal brines.
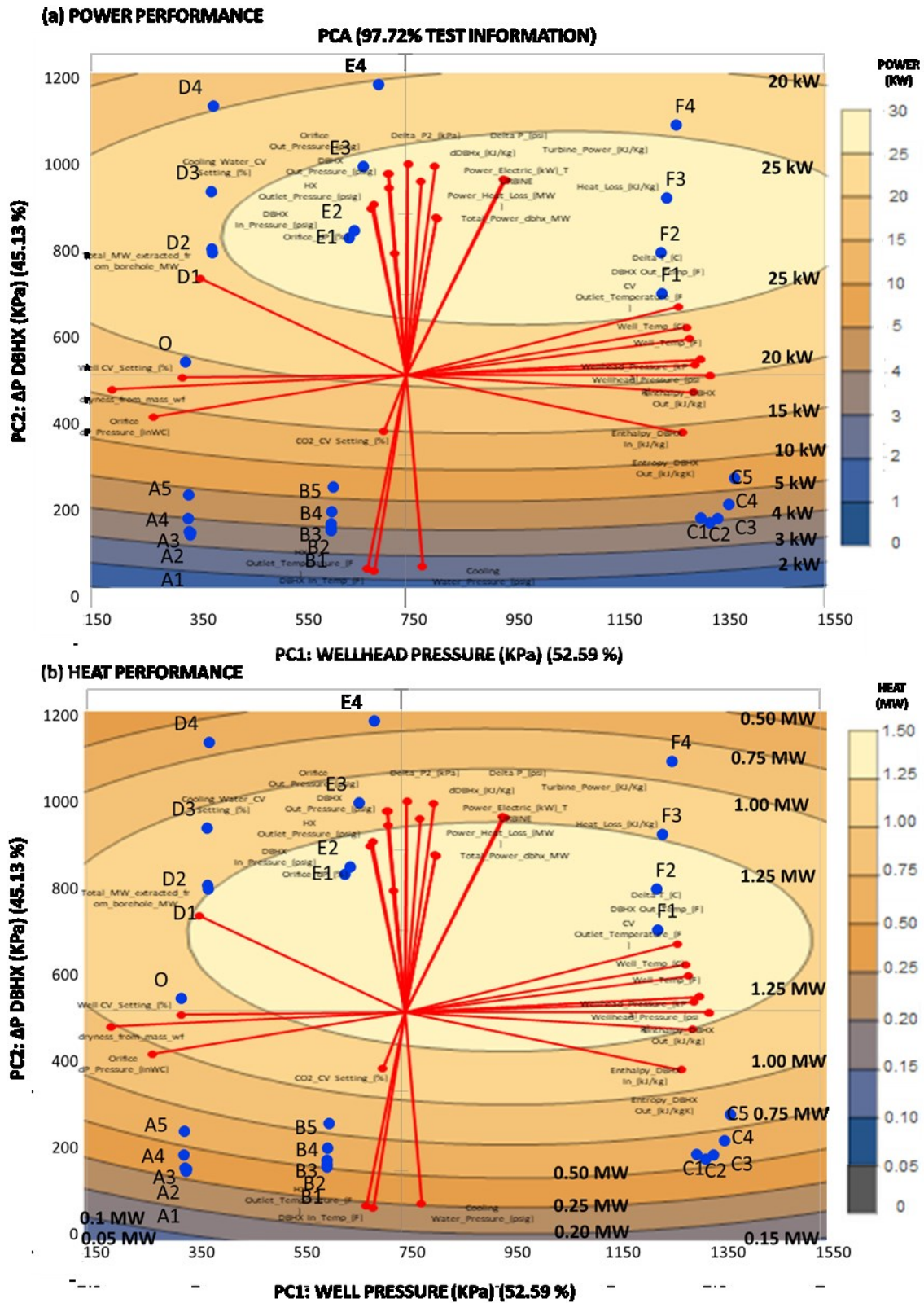
13

Figure 17: Principal Component axes ΔP DBHX sCO₂ vs. Wellhead Pressure and different experimental and variables setting conditions, (a) Electric Power contour overlaying the source plot and (b) Heat contour overlaying the source plot.
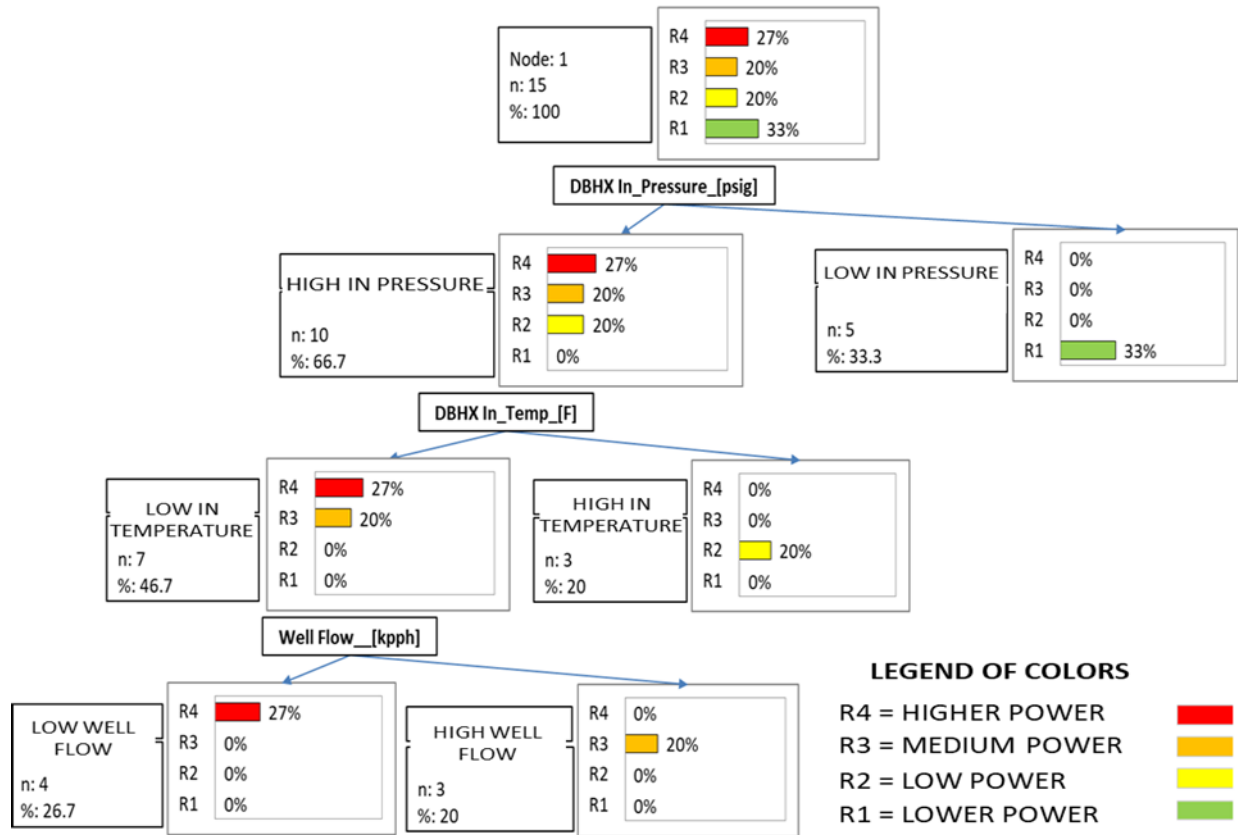
Figure 18: Decision tree chart for Power function optimization controlling DBHX inlet pressure, DBHX inlet temperature and Well Flow variables.

Figure 18 is a decision tree of variables that can be used to optimize power production through controlling some operational variables to work at specific conditions, such as DBHX inlet pressure, DBHX inlet temperature, and well flow levels. For example, in the December 2019 the inlet temperature was improved, producing more power. Bayesian technique was used to estimate intervals where power production can be optimized in the experimental variable domain of the (A_i-F_i) conditions. It shows after the first node that higher DBHX inlet pressure can discard the 33% of lower power production range (R1) in the histogram. At the next node, low DBHX inlet temperature can be used to discard the next 20% of low power production range (R2), which was already implemented in our December 2019 testing at a lower inlet temperature. At the next node, low well flow can be used to discard the next 20% range (R3), optimizing the 27% of remnant production range conditions (R4). However, if working in range R4 requires new equipment or investment, then a way to predict performance is to use statistical modeling to vary some cost-effective parameters before making an investment. Two of the variables that can optimize the power extraction and are going to be tested in the next analysis are the DBHX length and cooling temperature. First, they were synthetically varied using 1-D modeling equations (Figure 15) and then they were also used to forecast and extrapolate performance using a Monte Carlo simulation (Figure 19).

Finally, the fifth step of the statistical modeling is forecasting the total power expected considering the main operational variables and parameters of design using the Monte Carlo technique. One thousand resampling experiments were simulated considering the variation of DBHX length, DBHX flow and inlet temperature. The results (Figure 19) show that 104 kW can be obtained for a 1000 m of DBHX length and 31°C of cooling temperature for 7 kg/s of DBHX flow. However, any other scenario can be interpolated or extrapolated considering other conditions. The results of this section can be used in the future to continue optimizing conditions, designing and validating experiments and forecasting experiments, thereby avoiding the high cost of field-testing conditions. Figure 19a summarizes the probabilistic power production results, Figure 19b summarizes the DBHX sCO$_2$ flow (kg/s) forecasting distribution, Figure 19c summarizes the DBHX length (m) forecasting, and Figure 19d summarizes the inlet temperature (ºC) forecasting.
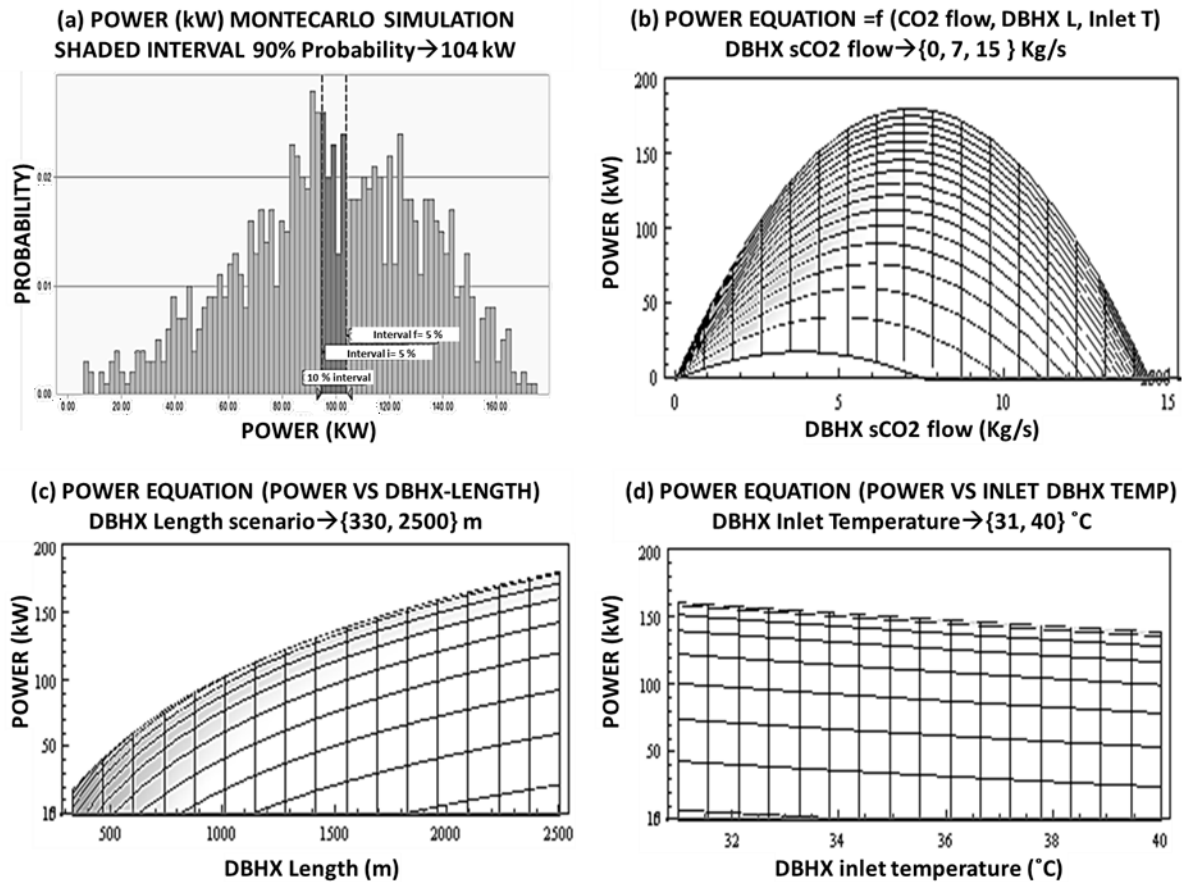
Figure 19: (a) Probabilistic power production results: power forecasting for 1000 iterations using Monte Carlo simulation and 1-D closed-loop modeling for 7 kg/s DBHX flow, 1000 m DBHX length, 31 ºC inlet temperature using triangular distributions of variables regarding experimental data and modeling results, (b) Power forecasting based on DBHX sCO$_2$ flow (kg/s), (c)Power forecasting based on DBHX length (m), (d) Power forecasting based on inlet DBHX temperature (ºC).

6. DIFFERENCES IN TESTING SCO$_2$ VERSUS WATER AS WORKING FLUID

According to the Coso demonstration results previously reported at Higgins et al. (2019), the closed-loop DBHX system installed at Coso geothermal field using water as the working fluid was able to deliver approximately 1 MW net power. For the case of sCO$_2$, the power delivered was around 10% of that produced with water. However, the tests and the results are not directly comparable for several key reasons: First, the sCO$_2$ flow rate was much lower than the water flow rate. In water experiments, the inlet flow was pumped at a rate that varied between 23 to 30 kg/s. In the case of the sCO$_2$ tests, the inlet flow was not pumped and resulted solely from the action of the thermosiphon so that the rate ranged between 1.5 to 5.5 kg/s, thereby delivering much less heat for power production. Second, since our calculations simulating the sCO$_2$ turbine used an isentropic efficiency assumption of 80% and the outlet pressure was restricted to be higher than the sCO$_2$ critical pressure (70 kPa), the power necessary for cooling and recompression was subtracted to obtain the net power. However, there was no actual compression of sCO$_2$ which, if it were to have occurred, would have produced higher flow and pressure at the turbine inlet, further increasing net power. In contrast, for the testing of water as the working fluid, power was calculated based on the pressure requirements of the geothermal power plant turbine. For these key reasons, and others relating to additional testing differences, a direct comparison between sCO$_2$ as the working fluid as described in this paper and water as the working fluid as described in the Higgins et al. (2019) paper, are not appropriate. However, both papers show that testing was successful in validating the modeling done in respect of the applicable working fluid which validation was the goal of each set of tests.

7. CONCLUSIONS

GreenFire Energy, with California Energy Commission, Shell GameChanger Program, Electric Power Research Institute (EPRI), and J-POWER funding, and with the strong support of the Coso Operating Company and the US Navy, has installed a demonstration downhole closed-loop heat exchanger into a well that has several megawatts of power production capability but contains prohibitively high NCG concentrations. This well was used to demonstrate closed-loop circulation of supercritical CO$_2$ without pumping. The circulation of the sCO$_2$ was entirely by a thermosiphon effect caused by cold (and dense) CO$_2$ flowing down an insulated pipe to the bottom of the DBHX. Upon the return to the surface, the sCO$_2$ absorbed heat and expanded greatly, thus preserving the pressure head built by the downflow dense column of sCO$_2$. The power production was not high, but verified GreenFire Energy's modeling and also,

notably, heat recovery was strong from DBHX considering that the sCO_2 flow rate was driven only by the thermosiphon and, consequently, low compared to recent testing with water as the working fluid. This result was expected since economic power production using sCO_2 generally requires several kilometers of depth to build up a sufficient pressure to produce 1 to 2 MW of electricity, driven only by the thermosiphon. A blower can be installed to increase power production, but that was outside the scope of this project.

A geothermal power coproduction relationship as a function of operational variables like control valve setting flows, inlet pressure, and inlet temperatures has been developed for sCO_2 as working fluid. This relationship was combined with the 1-D thermodynamic modeling results and Monte Carlo resampling results to develop a general equation that can be used to optimize power production in a wide range of experimental conditions by statistic modeling techniques. PCA analysis shows that in the range of experimental conditions tested at 330 m of length in this research, increasing DBHX inlet pressure, decreasing DBHX inlet temperature and decreasing brine well flow produces an optimization in power production in 77% of the cases.

The primary goal of the project has been to demonstrate the formation of a strong thermosiphon when circulating sCO_2 in a closed-loop system, and that it matches the modeling results. Verification of the modeling is essential before building a full-scale DBHX installation. Indeed, the modeling results successfully predict about the same production of power as was measured in the field.

8. FULL-SCALE APPLICATION OF ECO2G TO THE COSO GEOTHERMAL FIELD

One of the goals of this work has been to validate the 1-D modeling GreenFire Energy has developed inhouse to predict the performance of a DBHX for full-scale applications. In the full-scale application with sCO_2 as the working fluid (ECO2G), the DBHX is integrated directly into the well, with no annular region between the DBHX and the well casing. Heat is absorbed from the resource directly through the conduction of heat from the rock. Several architectures are possible, including, for improved performance, two wells connected at the bottom without the need to use a VIT (the sCO_2 goes down one well, and returns through the second connected well).

GreenFire Energy's modeling of full-scale ECO2G uses the same assumptions used in this paper, but includes the conductive heat transfer through the rock directly from the resource, and does not include geothermal brine flow around the DBHX. The methodology has been reviewed in a number of our previous papers (Fox and Higgins, 2016; and Higgins et al., 2016).

In Figure 20, we have plotted predicted power for a full-scale ECO2G system using the same modeling assumptions used in this paper. Since conduction through the rock is included in ECO2G modeling, we have used a thermal gradient and rock analysis appropriate for the Coso geology in our model, specifically, a non-permeable hard-rock geothermal resource with a thermal gradient of 120°C/km. The architecture modeled in Figure 20 is a vertical portion (3 or 4 km in depth) followed by a horizontal portion (0 to 6 km in length). The modeled system has a cemented outside casing that is 11-3/8 inches in diameter and is plugged at the bottom. Installed within this is a 6-5/8 inch diameter VIT. Generally, the vertical portion of the well is used to reach a sufficient depth for both high resource temperature and to develop a strong thermosiphon. The horizontal portion of the well is used to harvest heat from the resource into the sCO_2. Generally, longer and hotter well systems produce geometrically more power with ECO2G.
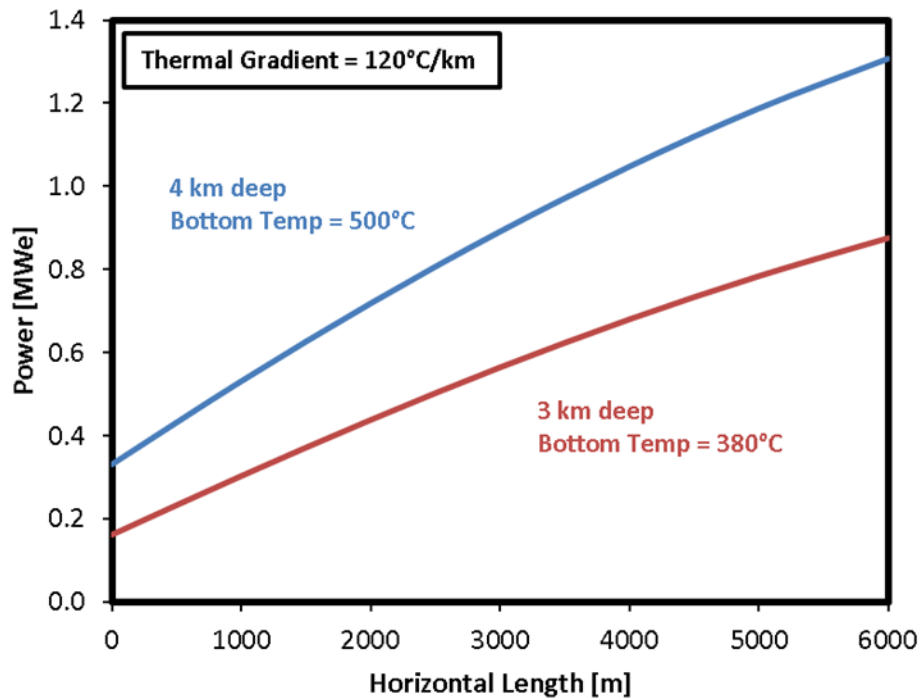
Figure 20: Power potential plotted versus horizontal length for a large diameter ECO2G system at various depths in a field with a thermal gradient of 120°C/km.

9. FUTURE WORK

Additional testing with supercritical sCO_2 as the working fluid is certainly merited. Measurements have been taken that will be used to determine closed-loop heat extraction capabilities when there is no well flow, which will simulate full-scale operation in hot, dry rock and enable fine-tuning the modeling techniques and assumptions.

Since the modeling approach appears to accurately capture the heat transfer in actual field testing, we will extend our modeling to consider other well and closed-loop configurations. For example, we intend to model performance with various well architectures, including fins and rods to increase the rate of heat transfer, and model performance with alternative DBHX diameters, lengths, and working fluids to optimize power production consistent with appropriate cost-benefit analysis.

Finally, most sCO_2 thermodynamic cycle applications use highly efficient turbines, high compressor capabilities and, sometimes, reboilers or combustion units before the turbine to increase the pressure. In the future, and given that our modeling of sCO_2 has now been verified with field testing, a complete techno-economic analysis considering this and many other configurations is warranted.

ACKNOWLEDGMENT

REFERENCES

Bell, Ian, Jorrit Wronski, Sylvain Quoilin, and Vincent Lemort. "Pure and Pseudo-pure Fluid Thermophysical Property Evaluation and the Open-Source Thermophysical Property Library CoolProp" *Ind. Eng. Chem. Res.* Vol 53, Issue 6, 2498-2508 (2014).

Bergman, Theodore L., Frank P. Incropera, and Adrienne S. Lavine. "Fundamentals of heat and mass transfer." John Wiley & Sons, (2011).

Fox, Don, and Brian Higgins. "The Effect of Well Density on Resource Depletion for a Vertical Closed-Loop sCO_2 Geothermal Well System," *Geothermal Resource Council Transactions*, Vol. 40 (2016).

Griffiths David, and Desmond Higham "Euler's Method. In: Numerical Methods for Ordinary Differential Equations" Springer Undergraduate Mathematics Series. Springer, London (2010).

Guo T., Gong F., Wang X., Lin Q., Qu Z., Zhang W., "Performance of enhanced geothermal system (EGS) in fractured geothermal reservoirs with CO_2 as working fluid", *Applied Thermal Engineering*, Vol. 152 (2019).

Haaland, S.E. "Simple and explicit formulas for the friction factor in turbulent pipe flow." *Journal of Fluids Engineering*, 105(1), 89-90 (1983).

Higgins, Brian S., Curtis M. Oldenburg, Mark P. Muir, Lehua Pan, and Alan D. Eastman, "Process Modeling of a Closed-Loop sCO$_2$ Geothermal Power Cycle," *The 5th International Supercritical CO$_2$ Power Cycles Symposium*, San Antonio, Texas, March 29 – 31 (2016).

Higgins; Brian S. Muir; John, Scherer; Joseph, Amaya; Alvaro, "GreenFire Energy Closed-Loop Geothermal Demonstration at the Coso Geothermal Field," *Geothermal Resource Council Transactions*, Vol. 43 (2019).

Kosukegawa H. and Fujii H., "Long-Term Heating Test Using the Semi-open Loop Ground Source Heat Pump System", *Proceedings 44th Workshop on Geothermal Reservoir Engineering*, Stanford University, Stanford, California, February 11-13 (2017).

Law R., Bridgland D., and Nicholson D., "Closed Loop Heat Extraction from Deep Single Wells," *Proceedings 41st Workshop on Geothermal Reservoir Engineering*, Stanford University, Stanford, California (2014).

Oldenburg C., Pan L., Muir M., Eastman A., and Higgins B., "Numerical Simulation of Critical Factors Controlling Heat Extraction from Geothermal Systems Using a Closed-Loop Heat Exchange Method," *Proceedings 43th Workshop on Geothermal Reservoir Engineering*, Stanford University, Stanford, California, (2016).

von Düring B., Campana F., and Ueing L., "An Innovative Concept for Geothermal Energy: The Closed Loop Technology Aiming for Zero Emissions," *European Geothermal Congress* (2016).

Yanagisawa N., Masuda Y., Osato K., Sato M., Kasai K., Sakura K., Fukui T., Akahori M., and Lichti K., "The material corrosion test using loop system under acidic conditions at geothermal field in Japan," *New Zealand Geothermal Workshop*. (2017).